Case Studies in Thermal Engineering 35 (2022) 102118

Contents lists available at ScienceDirect

Case Studies in Thermal Engineering

journal homepage: www.elsevier.com/locate/csite

Engine oil based MoS_2 Casson nanofluid flow with ramped boundary conditions and thermal radiation through a channel

Imran Siddique [a], Kashif Sadiq [a], Mohammed M.M. Jaradat [b,*], Rifaqat Ali [c], Fahd Jarad [d,e,f,**]

[a] Department of Mathematics, University of Management and Technology, Lahore, 54770, Pakistan
[b] Mathematics Program, Department of Mathematics, Statstics and Physics, College of Arts and Sciences, Qatar University, 2713, Doha, Qatar
[c] Department of Mathematics, College of Science and Arts, King Khalid University, Muhayil, 61413, Abha, Saudi Arabia
[d] Department of Mathematics, Cankaya University, Etimesgut, Ankara, Turkey
[e] Department of Mathematics, King Abdulaziz University, Jeddah, Saudi Arabia
[f] Department of Medical Research, China Medical University Hospital, China Medical University, Taichung, Taiwan

ARTICLE INFO

Keywords:
Casson nanofluid
Engine oil
MoS_2
Ramped wall conditions
Thermal radiation
Vertical channel

ABSTRACT

The modern era is a time to have cost-effective and energy-efficient technology. This demand has made nanotechnology the most effective field. The focus of this article is to increase the efficiency of engine oil (EO). The flow of EO-based Casson nanofluid containing Molybdenum disulfide (MoS_2) nanoparticles is investigated with ramped wall conditions and thermal radiation. Analytical results are calculated via the Laplace transform. The impact of physical parameters on isothermal and ramped conditions is illustrated graphically and discussed in detail. The researchers found that flow, mass, and energy can be controlled by using ramped conditions. The variation in concentration, temperature, and velocity is exponential for isothermal conditions and steady for ramped wall conditions. Finally, the results of Nusselt numbers, skin frictions, and Sherwood numbers on both walls of the channel for both isothermal and ramped conditions are graphically depicted and discussed. For higher values of time the results of ramped and isothermal wall conditions are identical. It is found that the nanoparticles of MoS_2 enhance the lubrication and heat transport rates of EO.

Nomenclature

$\widetilde{C}(\widetilde{y},\widetilde{t})$	Concentration (kg m-3)
$\widetilde{u}(\widetilde{y},\widetilde{t})$	Velocity (m s^{-1})
$\widetilde{T}(\widetilde{y},\widetilde{t})$	Temperature (K)
k	Thermal Conductivity (W m-1 K-1)
g	Gravitational acceleration (m s-2)
D	Mass diffusivity (m^2 s^{-1})

* Corresponding author. Mathematics Program, Department of Mathematics, Statistics and physics, College of Arts and sciences, Qatar University, Doha, Qatar.
** Corresponding author. Department of Mathematics, Cankaya University, Etimesgut, Ankara, Turkey.
E-mail addresses: imransmsrazi@gmail.com (I. Siddique), kashifsadiq2525@gmail.com (K. Sadiq), mmjst4@qu.edu.qa (M.M.M. Jaradat), rrafat@kku.edu.sa (R. Ali), fahd@cankaya.edu.tr (F. Jarad).

https://doi.org/10.1016/j.csite.2022.102118
Received 19 March 2022; Received in revised form 3 May 2022; Accepted 13 May 2022
Available online 17 May 2022

Gr	Thermal Grashof number
Pr	Prandtl number
cp	Specific heat (J kg-1 K-1)
Gm	Mass Grashof number
R	Chemical reaction (s^{-1})
Sc	Schmidt number
Nu	Nusselt number
Sk	Skin friction
Sh	Sherwood number

Greek Symbols

θ	Dimensionless temperature
μ	Dynamic Viscosity (kg m^{-1} s^{-1})
ρ	Density (kg m^{-3})
βT	Thermal expansion (K^{-1})
φ	Nanoparticles volume fraction
ν	Kinematic viscosity (m^2 s^{-1})
βC	Mass volumetric (K^{-1})
γ	Casson Parameter

Subscript

f	Fluid
nf	Nanofluid
s	Solid particles

1. Introduction

Non-Newtonian fluids are attracting researchers due to their applications in the industrial and technological sciences. Sugar solutions, blood, clay coating, paints, drilling mud, certain oils, and synthetic lubricants are different types of non-Newtonian fluids. These fluids cannot be defined by the Navier-Stokes equations due to their complex mathematical formulation. Jeffrey, Burger, Casson, Carreau, Maxwell, Oldroyd-B, Seely, Bulky and Eyring-Powell fluids are modeled to classify various non-Newtonian fluids according to their characteristics. The model of Casson [1] fluid helped to understand the features of dying oil deferments of ink used for printing. Casson fluids are shear-thinning fluids [2] and have infinite viscosity at zero shear stress and zero viscosity at infinite shear stress. Human blood, soup, honey, tomato sauce, and jelly are different Casson fluids.

For the last two decades, researchers have been investigating nanofluids due to their extraordinary characteristics. Conventional fluids like engine oil, water, ethylene glycol, sodium alginate, and kerosene oil have significant use in the application of heat transfer, but these reduce the rate of heat transport due to low thermal conductivities. The nanofluids are useful to save energy and reduce the temperature of the equipment [3–6]. For instance, the most common uses of nanofluids are as lubricants in the transportation of heavy machines, biomedical tools, heat exchangers, food processing, fuel cells, biomedicine, computer microchips, and coolants in automobiles [7,8]. Loganathan et al. [9] established the first analytical solution of convective nanofluid flow with radiation. The characteristics of carbon nanotubes in a fluid affected by partial slip were investigated by Reddy et al. [10]. Archana et al. [11] studied the incompressible and compressed flow of Casson nanofluid, which is used as a lubricant, between two parallel plates. The constitutive equations are included in the mathematical formulation. Reddy et al. [12] explored magnetohydrodynamic flow, thermal conduction, and diffusion nanofluid flow over a stretched sheet.

To increase heat transport properties, a term called “hybrid nanofluid”, which is a novel form of nanofluid, has recently been used. Solar cells, power generation engines, cooling devices, naval structures, medical, defense, transportation, and micro-fluidics are a few examples of nanofluids. Reddy et al. [13] examined the hybrid nanofluid flow across a revolving disc. Kumar et al. [14] used hybrid nanofluids to investigate the sustainability of heat transport increases caused by major characteristics variations of nanofluids under the influence of thermal radiation. Reddy et al. [15] used the Koo and Kleinstreuer model to examine the Blasius and Rayleigh-Stokes flow of aluminium alloys across a semi-infinite heated plate in Darcy-Forchheimer porous space under the impact of nonlinear radiation. Souayeh [16] established a mathematical model for dusty hybrid nanofluid flow and heat transmission across a stretched sheet. An incompressible two-dimensional flow of hybrid dusty nanofluid in a Darcy-Forchheimer medium on a stretched sheet was studied by Reddy et al. [17]. Kumar et al. [18] investigated the nature of a moving frame hydrodynamic hybrid nanofluid by applying solar radiation.

The EO is used as a lubricant and has significant applications in the mechanical, chemical, and production industries. Meng et al. [19] investigated EO-silver nanofluid. Eswaraiah et al. [20] analyzed the results of the EO-graphene nanofluid. Aman et al. [21] calculated the analytical results of Maxwell nanofluid (MoS_2-EO) flow. Arif et al. [22] discussed the applications of EO-based nanofluids. The use of nanoparticles of various shapes helps to improve the efficiency of lubricants. The nanoparticles of MoS_2 are added to EO due to its robustness and low friction, which boost the lubricity and thermal conductivity of EO [23,24]. MoS_2 is a black, silvery solid that appears as the mineral molybdenite and contains atoms of sulphur and molybdenum and is classified in the class of inorganic

compounds. MoS_2 is comparatively unaffected and nonreactive by dilute oxygen and acids. Zhang et al. [25] experimentally prepared stable MoS_2 nanofluids. The major attraction of MoS_2 for researchers is its applications, mainly in two-dimensional (2D) electronic machines like amplifiers, logic circuits, and field-effect transistors [26,27]. Researchers also investigated factors like volumetric expansion, thermal conductivity, and heat capacity [28–33].

The use of ramped wall conditions is very significant in different sections of modern science and technology. For example, ramped velocity helps to evaluate the functioning of blood vessels and the heart, to diagnose blood-vascular diseases, and to determine treatment and find prognosis involving treadmill ergometry [34]. Despite the practical propositions, not enough study is done with ramped conditions. Ramped conditions play a vital role in managing the flow, mass, and energy of the fluid. Ahmed and Dutta [35] introduce ramped velocity and temperature for Newtonian fluid flow on a vertical moving plate. Ali et al. [36], Seth et al. [37] and Kao [38], they studied the impact of ramped wall temperature on diverse physical phenomena of modern science and found the results. Seth et al. [39–41] discussed mass and heat transport under the effect of ramped heating. Chandran et al. [42] analyzed mixed convection flow with ramped heating. Arif et al. [43] examined the EO-based fractionalized Casson fluid containing nanoparticles of graphene oxide and MoS2 with ramped heating and ramped concentration.

The movement of machine parts produces additional heat owing to frictional forces in various operating systems, causing machine components to be unable to continue their functions and stop working before time. We have worked to develop the most significant qualities of lubricants for machines, such as EO, so that they can have a long service life and work for longer periods of time. Additives are critical components in oils and greases, as well as in the long-term performance of bearings and other machine components. Keeping these theories in mind, MoS_2 nanoparticles are used in the current investigation. The rate of heat transfer will be enhanced without reducing the thickness of EO. As a consequence, the life of machineries such as bearings, automotive engines, and turbines will be extended, and they will operate more efficiently. In the above literature, most of the investigations are on ramped temperature, and in very few, ramped concentration is included. There is no evidence of the results of the Casson nanofluid flow with ramped velocity. Also, most of the studies are for the flow on a single plate. Here the motivation is to discuss the flow of EO-MoS_2 Casson nanofluid in the channel with ramped wall conditions and thermal radiation. The particles of MoS_2 are dispersed in EO to prepare a nanofluid. Analytical results are calculated via the Laplace transform. The influence of physical parameters on isothermal and ramped conditions is depicted graphically and explained.

2. Mathematical model

Consider an incompressible, unsteady flow of Casson nanofluid inside two infinite vertical parallel plates (walls) with ramped boundary conditions and thermal radiation. Nanoparticles of MoS_2 are suspended in EO to have a nanofluid.

At $t^* = 0$ ($y^* = 0$ and$y^* = l$), the temperature, velocity, and concentration are uniform. At $0 < t^* < {t_0}^*$, the temperature, concentration, and velocity of left plate change temporarily to ${T_l}^* + ({T_0}^* - {T_l}^*){t^*}/{t_0}^*$, ${C_l}^* + ({C_0}^* - {C_l}^*){t^*}/{t_0}^*$, and ${u_0}{t^*}/{t_0}^*$, respectively. After $y^* = l$, the system attains its initial position (see Fig. 1). We have made the following assumptions:

- Nanofluid is considered optically thick. Therefore the Rosseland approximations can be considered for radiation effects.
- The flow is being confined to $y^* > 0$.
- For $t^* > 1$, the ramped wall conditions changes to isothermal conditions.
- Velocity, concentration, and temperature are functions of y^* and t^* only.

Thermo-physical features of EO and MoS_2 are assumed constant and shown in Table 1.
The governing Eqs. are [43,44]:

$$u^*(0,t^*) = \begin{cases} u_0 \dfrac{t^*}{t_0^*}, & 0 < t^* \le t_0^* \\ u_0, & t^* > t_0^* \end{cases}$$

$$T^*(0,t^*) = \begin{cases} T_l^* + \left(T_0^* - T_l^*\right)\dfrac{t^*}{t_0^*}, & 0 < t^* \le t_0^* \\ T_0^*, & t^* > t_0^* \end{cases}$$

$$C^*(0,t^*) = \begin{cases} C_l^* + \left(C_0^* - C_l^*\right)\dfrac{t^*}{t_0^*}, & 0 < t^* \le t_0^* \\ C_0^*, & t^* > t_0^* \end{cases}$$

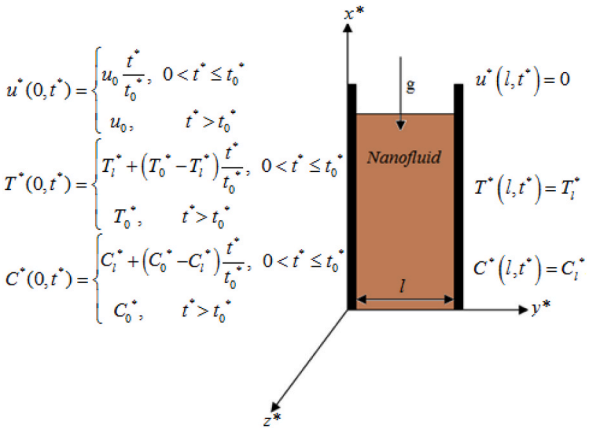

Fig. 1. Flow geometry.

Table 1
Thermo-physical properties of EO and MoS_2 [43].

Material	ρ	k	$\beta \times 10^{-5}$	c_p
Engine oil (EO)	884	0.144	70	1910
MoS_2	5600	904.4	2.8424	397.21

$$\rho_{nf}\frac{\partial u^*(y^*,t^*)}{\partial t^*}=\mu_{nf}\left(1+\frac{1}{\gamma}\right)\frac{\partial^2 u^*(y^*,t^*)}{\partial y^{*2}}+g(\rho\beta_C)_{nf}(C^*(y^*,t^*)-C_l^*)+g(\rho\beta_T)_{nf}(T^*(y^*,t^*)-T_l^*), \tag{1}$$

$$(\rho c_p)_{nf}\frac{\partial T^*(y^*,t^*)}{\partial t^*}=k_{nf}\frac{\partial^2 T^*(y^*,t^*)}{\partial y^{*2}}-\frac{\partial q_r}{\partial y^*}, \tag{2}$$

$$\frac{\partial C^*(y^*,t^*)}{\partial t^*}=D_{nf}\frac{\partial^2 C^*(y^*,t^*)}{\partial y^{*2}}, \tag{3}$$

with corresponding conditions are [45]:

$$u^*(y^*,0)=0, T^*(y^*,0)=T_l^*, C^*(y^*,0)=C_l^*, 0\le y^*\le l, \tag{4}$$

$$u^*(0,t^*)=\begin{cases}u_0\dfrac{t^*}{t_0^*}, & 0<t^*\le t_0^*;\\ u_0, & t^*>t_0^*\end{cases}, T^*(0,t^*)=\begin{cases}T_l^*+(T_0^*-T_l^*)\dfrac{t^*}{t_0^*}, & 0<t^*\le t_0^*;\\ T_0^*, & t^*>t_0^*\end{cases},$$
$$C^*(0,t^*)=\begin{cases}C_l^*+(C_0^*-C_l^*)\dfrac{t^*}{t_0^*}, & 0<t^*\le t_0^*;\\ C_0^*, t^*>t_0^*\end{cases}, \tag{5}$$

$$u^*(l,t^*)=0, T^*(l,t^*)=T_l^*, C^*(l,t^*)=C_l^*. \tag{6}$$

The characteristics of nanofluids are [46,47]:

$$\frac{\mu_{nf}}{\mu_f}=\frac{1}{(1-\varphi)^{2.5}}, \frac{\rho_{nf}}{\rho_f}=\varphi\frac{\rho_s}{\rho_f}+(1-\varphi), \frac{(\rho c_p)_{nf}}{(\rho c_p)_f}=\varphi\frac{(\rho c_p)_s}{(\rho c_p)_f}+(1-\varphi), \tag{7}$$

$$\frac{(\rho\beta_T)_{nf}}{(\rho\beta_T)_f}=\varphi\frac{(\rho\beta_T)_s}{(\rho\beta_T)_f}+(1-\varphi), \frac{(\rho\beta_C)_{nf}}{(\rho\beta_C)_f}=\varphi\frac{(\rho\beta_C)_s}{(\rho\beta_C)_f}+(1-\varphi), \tag{8}$$

$$\frac{D_{nf}}{D_f}=(1-\varphi), k_{nf}=k_f\frac{\left[2k_f+k_s-2\varphi(k_f-k_s)\right]}{\left[2k_f+k_s+\varphi(k_f-k_s)\right]}. \tag{9}$$

Non-dimensional variables, functions, and parameters are

$$u=\frac{u^*}{u_0}, t=\frac{t^*}{t_0^*}, t_0^*=\frac{l^2}{\nu_f}, y=\frac{y^*}{l}, \theta=\frac{T^*-T_l^*}{T_0^*-T_l^*}, C=\frac{C^*-C_l^*}{C_0^*-C_l^*}, \alpha_1=\frac{\rho_f}{\rho_{nf}(1-\varphi)^{2.5}}\left(1+\frac{1}{\gamma}\right),$$
$$\alpha_2=Gr\frac{(\beta_T)_{nf}}{(\beta_T)_f}, \alpha_3=Gm\frac{(\beta_C)_{nf}}{(\beta_C)_f}, \alpha_4=\frac{1}{\Pr}\left(\frac{k_{nf}}{k_f}+Nr\right)\frac{(\rho c_p)_f}{(\rho c_p)_{nf}}, \alpha_5=\frac{1-\varphi}{Sc}, \tag{10}$$
$$Gm=\frac{g(\beta_C)_f(C_0-C_l)d^2}{U_0\nu_f}, Gr=\frac{g(\beta_T)_f(T_0-T_l)d^2}{U_0\nu_f}, \Pr=\frac{(\rho c_p)_f\nu_f}{k_f}, Sc=\frac{\nu_f}{D_f}.$$

By substituting Eq. (10) to Eqs. (1)–(6), we get

$$\frac{\partial u(y,t)}{\partial t}=\alpha_1\frac{\partial^2 u(y,t)}{\partial y^2}+\alpha_2\theta(y,t)+\alpha_3 C(y,t), \tag{11}$$

$$\frac{\partial\theta(y,t)}{\partial t}=\alpha_4\frac{\partial^2\theta(y,t)}{\partial y^2}, \tag{12}$$

$$\frac{\partial C(y,t)}{\partial t} = \alpha_5 \frac{\partial^2 C(y,t)}{\partial y^2}. \tag{13}$$

$$u(y,0) = \theta(y,0) = C(y,0) = 0; \quad 0 \le y \le 1, \tag{14}$$

$$u(0,t) = \theta(0,t) = C(0,t) = \begin{cases} t, & 0 < t \le 1; \\ 1, & t > 1 \end{cases} = H(t)t - H(t-1)(t-1), \tag{15}$$

$$u(1,t) = \theta(1,t) = C(1,t) = 0. \tag{16}$$

3. Solution of the problem

Applying Laplace transform to Eqs. 11–13,(15), (16) and using(14), we obtain

$$\alpha_1 \frac{\partial^2 \overline{u}(y,\tau)}{\partial y^2} - \tau \overline{u}(y,\tau) = -\alpha_2 \overline{\theta}(y,\tau) - \alpha_3 \overline{C}(y,\tau), \tag{17}$$

$$\alpha_4 \frac{\partial^2 \overline{\theta}(y,\tau)}{\partial y^2} - \tau \overline{\theta}(y,\tau) = 0, \tag{18}$$

$$\alpha_5 \frac{\partial^2 \overline{C}(y,\tau)}{\partial y^2} - q \overline{C}(y,\tau) = 0, \tag{19}$$

and

$$\overline{u}(0,\tau) = \overline{\theta}(0,\tau) = \overline{C}(0,\tau) = \tau^{-2}(1-e^{-\tau}),\ \overline{u}(1,\tau) = \overline{\theta}(1,\tau) = \overline{C}(1,\tau) = 0. \tag{20}$$

The solution of Eqs. 17–19 subject to Eq. (20), gives

$$\begin{aligned} \overline{u}(y,\tau) = (1-e^{-\tau}) \Bigg[& \left(\frac{1}{\tau} + \frac{\alpha_2\alpha_4}{(\alpha_1-\alpha_4)\tau^2} + \frac{\alpha_3\alpha_5}{(\alpha_1-\alpha_5)\tau^2} \right) \frac{\sinh\left[(1-y)\sqrt{\frac{\tau}{\alpha_1}}\right]}{\tau \sinh\left[\sqrt{\frac{\tau}{\alpha_1}}\right]} \\ & - \frac{\alpha_2\alpha_4}{(\alpha_1-\alpha_4)\tau^2} \frac{\sinh\left[(1-y)\sqrt{\frac{\tau}{\alpha_4}}\right]}{\tau \sinh\left[\sqrt{\frac{\tau}{\alpha_4}}\right]} - \frac{\alpha_3\alpha_5}{(\alpha_1-\alpha_5)\tau^2} \frac{\sinh\left[(1-y)\sqrt{\frac{\tau}{\alpha_5}}\right]}{\tau \sinh\left[\sqrt{\frac{\tau}{\alpha_5}}\right]} \Bigg], \end{aligned} \tag{21}$$

$$\overline{\theta}(y,\tau) = (1-e^{-\tau}) \frac{\sinh\left[(1-y)\sqrt{\frac{\tau}{\alpha_4}}\right]}{\tau^2 \sinh\left[\sqrt{\frac{\tau}{\alpha_4}}\right]}. \tag{22}$$

$$\overline{C}(y,\tau) = (1-e^{-\tau}) \frac{\sinh\left[(1-y)\sqrt{\frac{\tau}{\alpha_5}}\right]}{\tau^2 \sinh\left[\sqrt{\frac{\tau}{\alpha_5}}\right]}. \tag{23}$$

The inverse Laplace transform of Eqs. 21–23, gives

$$u(y,t) = u_0(y,t) - H(t-1)u_0(y,t-1), \tag{24}$$

$$\theta(y,t) = \sum_{n=0}^{\infty} \int_0^t f(y,\alpha_4,\tau)d\tau - H(t-1) \sum_{n=0}^{\infty} \int_0^t f(y,\alpha_4,\tau-1)d\tau, \tag{25}$$

$$C(y,t) = \sum_{n=0}^{\infty} \int_0^t f(y,\alpha_5,\tau)d\tau - H(t-1) \sum_{n=0}^{\infty} \int_0^t f(y,\alpha_5,\tau-1)d\tau, \tag{26}$$

where

$$u_0(y,t)=\sum_{n=0}^{\infty}\int_0^t\left(1+\frac{\alpha_2\alpha_4\tau}{(\alpha_1-\alpha_4)}+\frac{\alpha_3\alpha_5\tau}{(\alpha_1-\alpha_5)}\right)f(y,\alpha_1,t-\tau)d\tau$$
$$-\frac{\alpha_2\alpha_4}{(\alpha_1-\alpha_4)}\sum_{n=0}^{\infty}\int_0^t(t-\tau)f(y,\alpha_4,\tau)d\tau-\frac{\alpha_3\alpha_5}{(\alpha_1-\alpha_5)}\sum_{n=0}^{\infty}\int_0^t(t-\tau)f(y,\alpha_5,\tau)d\tau, \tag{27}$$

and

$$F(y,\alpha_k,q)=\frac{\sinh\left(\frac{(1-y)}{\sqrt{\alpha_k}}\sqrt{q}\right)}{q\sinh\left(\frac{1}{\sqrt{\alpha_k}}\sqrt{q}\right)}=\sum_{n=0}^{\infty}\left[\frac{e^{-\frac{(2n+y)}{\sqrt{\alpha_k}}\sqrt{q}}}{q}-\frac{e^{-\frac{(2n+2-y)}{\sqrt{\alpha_k}}\sqrt{q}}}{q}\right],\ k=1,4,5. \tag{28}$$

$$f(y,\alpha_k,t)=erfc\left(\frac{2n+y}{2\sqrt{\alpha_k t}}\right)-erfc\left(\frac{2n+2-y}{2\sqrt{\alpha_k t}}\right),\ k=1,4,5. \tag{29}$$

4. Nusselt numbers, skin friction, and Sherwood numbers

The Nusselt numbers, skin frictions, and Sherwood numbers on both walls of the channel can express as [43,48].

$$Nu_{0,1}=-\frac{k_{nf}}{k_f}\frac{\partial\theta(y,t)}{\partial y}\bigg|_{y=0,1}. \tag{30}$$

$$Sk_{0,1}=-\frac{\mu_{nf}}{\mu_f}\left(1+\frac{1}{\gamma}\right)\frac{\partial u(y,t)}{\partial y}\bigg|_{y=0,1}. \tag{31}$$

$$Sh_{0,1}=-\frac{D_{nf}}{D_f}\frac{\partial C(y,t)}{\partial y}\bigg|_{y=0,1}. \tag{32}$$

5. Graphical results and discussions

The flow of EO-MoS_2 nanofluid is analyzed graphically in the section. Figs. 2–4 show the impacts of variation of physical parameters volume fraction (φ), Casson parameter (γ), Schmidt number (Sc), Prandtl number (Pr) and Grashof numbers (Gr and Gm) on non-dimensional velocity, concentration, and temperature fields. Furthermore, the figures also show the comparison of results for both ramped and isothermal conditions. The results of ramped boundary conditions are applicable for time $0<t<1$, isothermal conditions are suitable for time $t>1$. The results show that the variations with ramped conditions are steady compare to isothermal conditions, which are exponential. For higher values of time ($t>1$) the results of ramped and isothermal wall conditions are identical.

Figs. 2(a), 3(a) and 4(a) show how φ affects concentration, energy, and momentum profiles. The concentration and velocity profiles are decreasing due to the thickness caused by the higher density of MoS_2 particles, the temperature of the nanofluid rises due to the superior thermal conductivity of MoS_2. Fig. 2(b) illustrates that the concentration decreases by increasing Sc.

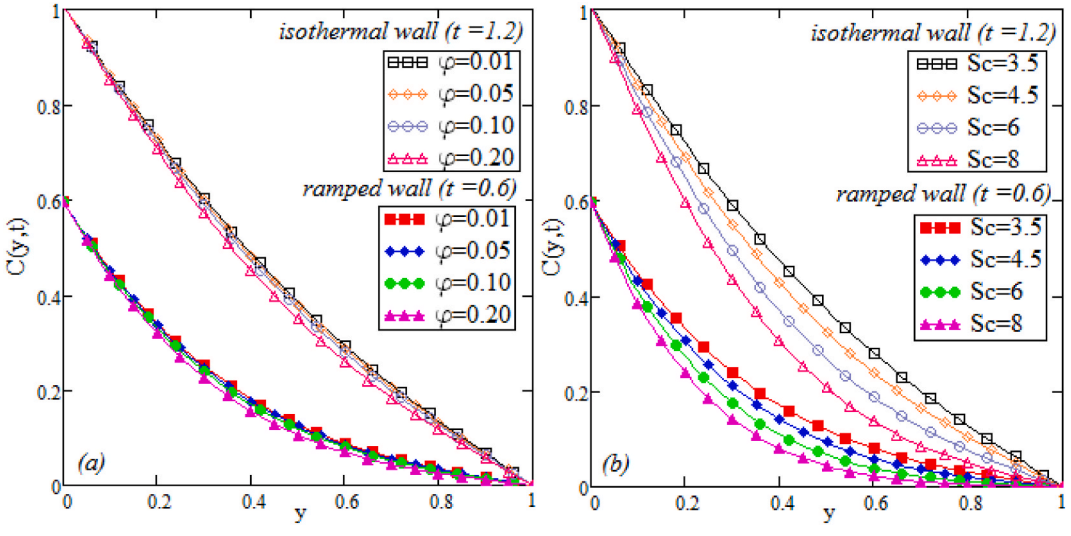

Fig. 2. Variation of concentration when.$Sc=3.3, \varphi=0.04$.

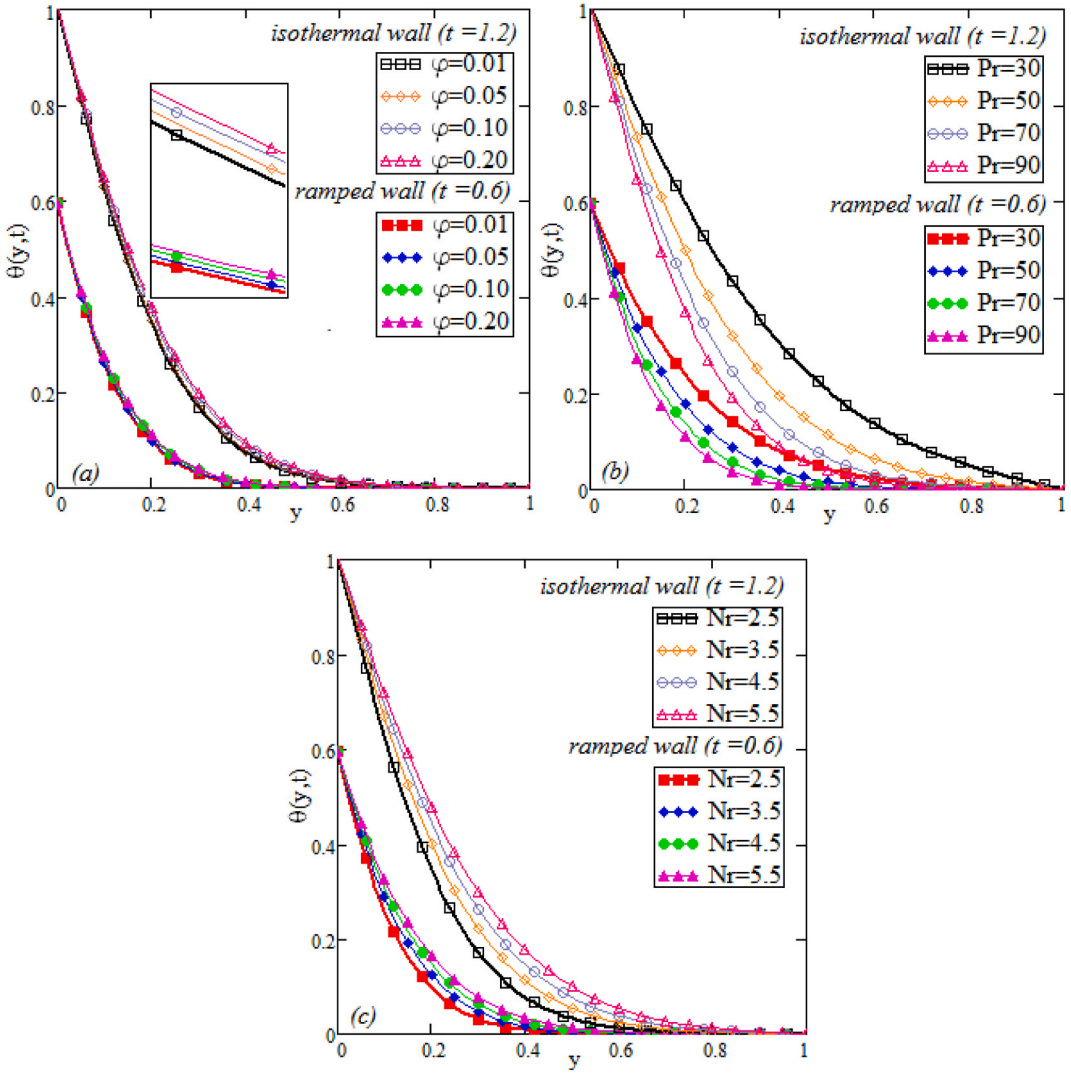

Fig. 3. Variation of temperature when.$\varphi = 0.04, \mathrm{Pr} = 100, Nr = 2.5$.

Fig. 3(b) illustrates that the viscosity of the nanofluid rises for greater values of Pr which reduces the temperature. Fig. 3(c) demonstrates that the increase in temperature at higher thermal radiation. Fig. 4(b) and (c) show the influence of buoyancy forces (*Gr* and *Gm*) on velocity. The rise in these forces increases the flow of the nanofluid. The influence of γ on the velocity profile is seen in Fig. 4(d). For increasing values of γ, the velocity increases exponentially for the isothermal conditions and steadily for the ramped conditions. With ramped and isothermal conditions, flow, energy, and concentration are compared. It has been proven that ramped velocity, concentration, and temperature are less than those obtained under isothermal circumstances. As a result, the ramped wall conditions are more suitable.

Fig. 5 depicts the rate of heat transport on both walls of the channel with isothermal and ramped conditions. An exponential rise is found in heat transfer by increasing. φ.

Fig. 6 demonstrates the fluctuation of skin frictions on both walls of the channel with isothermal and ramped conditions. An increase in skin friction is noticed by increasing. φ.

Fig. 7 illustrates the rate of mass transport on both walls of the channel with isothermal and ramped conditions. The rate of mass transfer increases by increasing. φ.

Fig. 8 illustrates the comparison of present results with existing results of Kashif et al. [45]. It is concluded that in the absence of chemical reactions (K, R), heat generation (Q), thermal radiation (Nr), and Casson Parameter $(\gamma \to \infty)$ the results are identical.

6. Conclusions

Analytical results are calculated via the Laplace transform. The influence of physical parameters on isothermal and ramped conditions is illustrated graphically and discussed in detail. The researchers found that flow, mass, and energy can be controlled by using

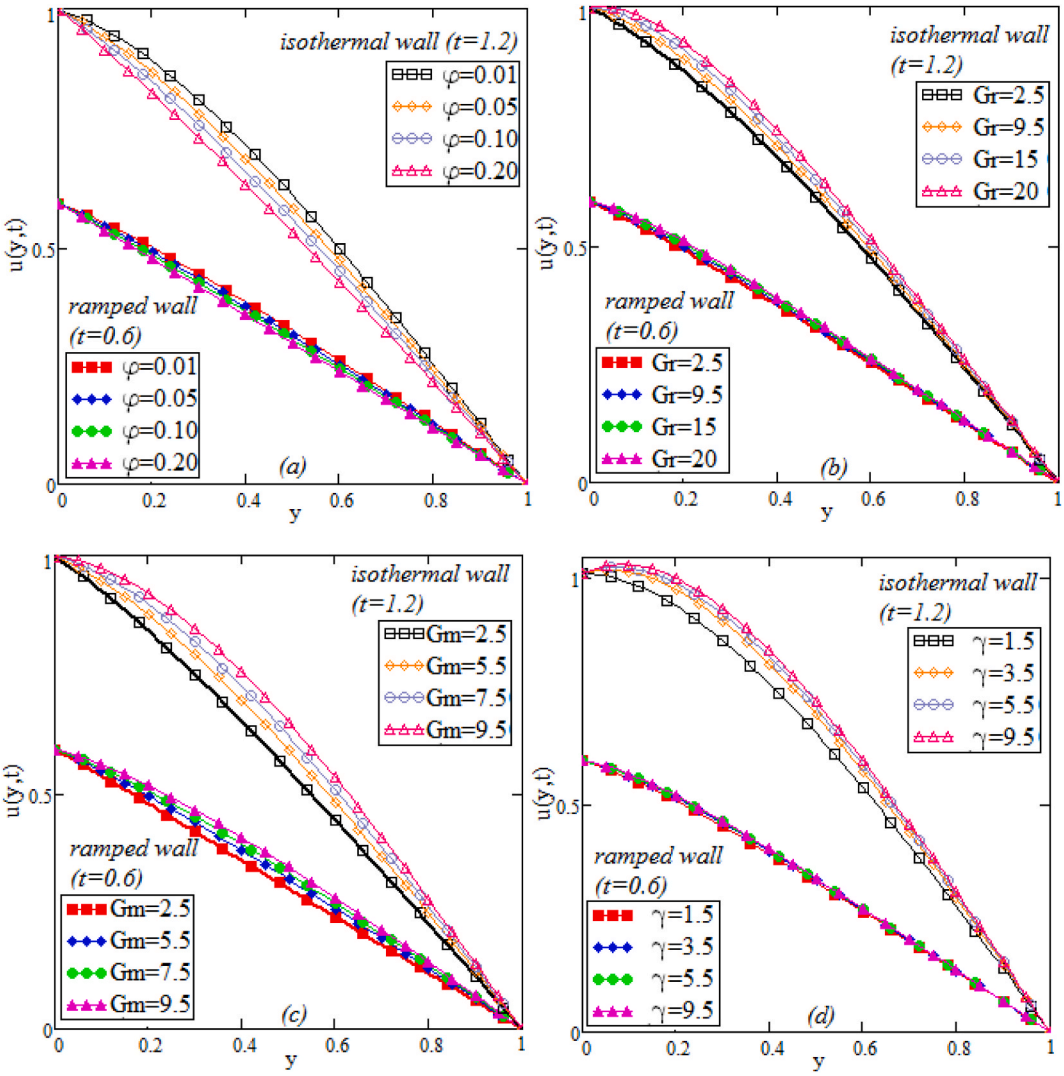

Fig. 4. Variation of velocity when.$\varphi = 0.04, Gr = 4.5, \Pr = 100, Sc = 1.3, \gamma = 0.5, Gm = 5.2, Nr = 2.5$.

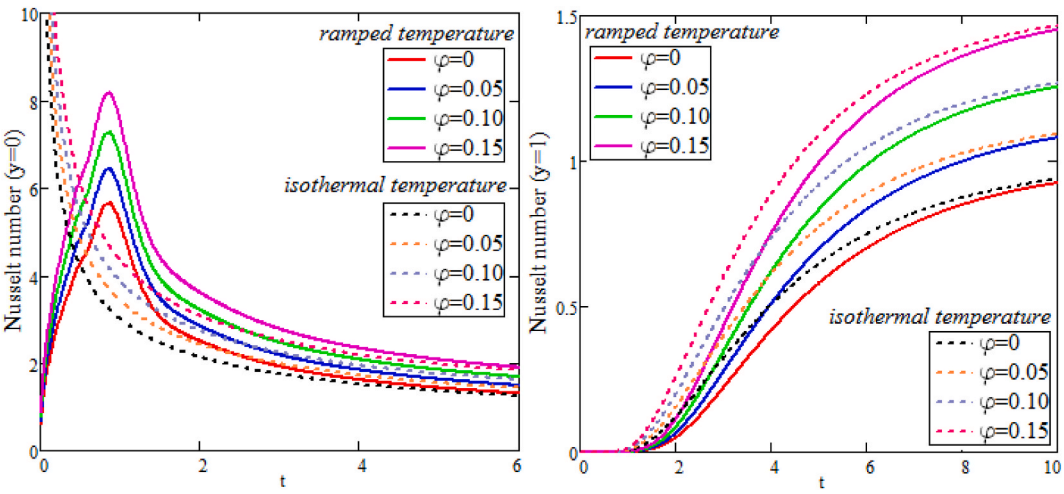

Fig. 5. Effects of φ on Nusselt numbers when.$\Pr = 100, Nr = 2.5$.

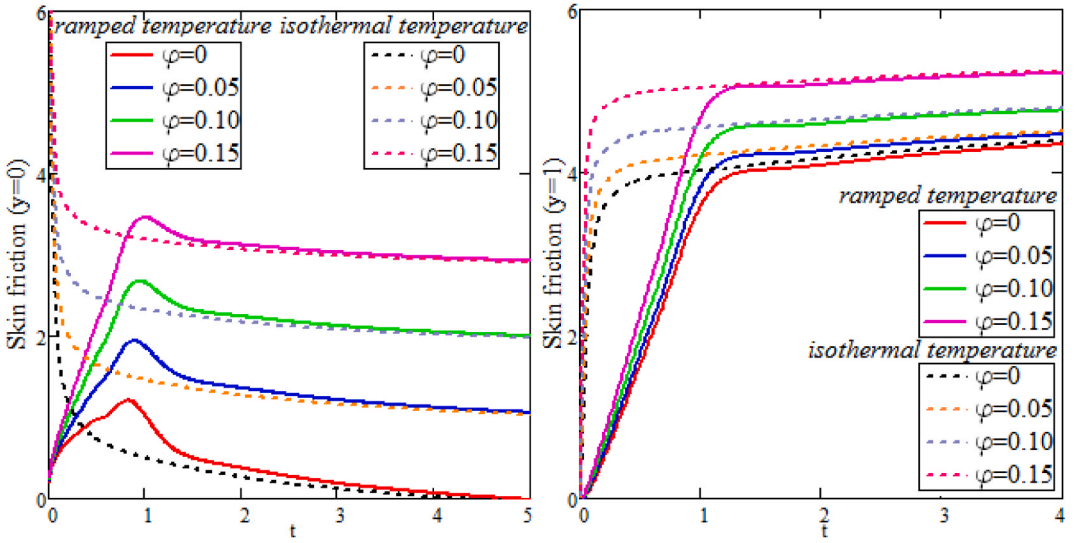

Fig. 6. Effects of φ on skin frictions when.$Gr = 4.5, \Pr = 100, Sc = 1.3, \gamma = 0.5, Gm = 5.2, Nr = 2.5$.

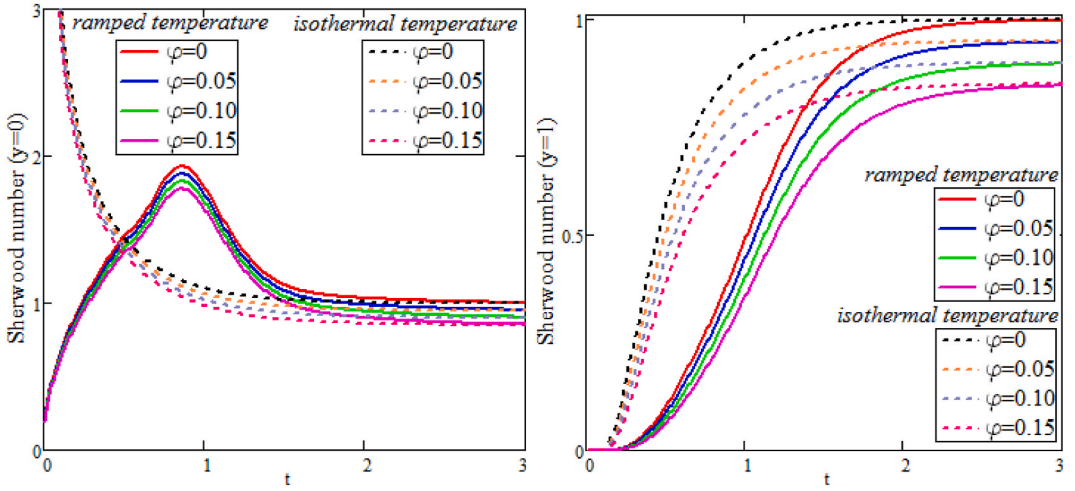

Fig. 7. Effects of φ on Sherwood numbers when.$Sc = 3.3$.

ramped conditions. The variation in concentration, temperature, and velocity is exponential for isothermal boundary conditions and steady for ramped conditions. Finally, the results of Nusselt numbers on both walls (y = 0 and y = 1) of the channel for both ramped conditions and isothermal conditions are graphically depicted and discussed. MoS_2 nanoparticles enhance the lubrication and heat transport rates of EO. An integral transform (Laplace) is used to calculate the results. A nanofluid is prepared by adding nanoparticles of MoS_2 to EO. The noteworthy outcomes for velocity, concentration, temperature, and Nusselt numbers for both ramped and isothermal conditions are graphically highlighted and explained in depth.

The following are the most important outcomes of this research:

- Isothermal boundary conditions have higher concentrations, speeds, and temperatures than ramped boundary conditions.
- Ramped conditions reduce the Casson parameter's effect.
- With ramped wall conditions, variations in concentration, velocity, and temperature fields can be controlled.
- For increasing values of γ, Gr, Gm, the velocity field rises, while for increasing values of φ, the velocity field decreases.
- As Pr grows, the temperature drops, and as φ rises, the temperature increases.
- As Sc increases, the concentration of the ramped wall decreases.
- The Nusselt numbers skin frictions rise with the rise of φ.
- The Sherwood numbers decrease with the increase of φ.
- For higher values of t the results of ramped and isothermal wall conditions are identical.

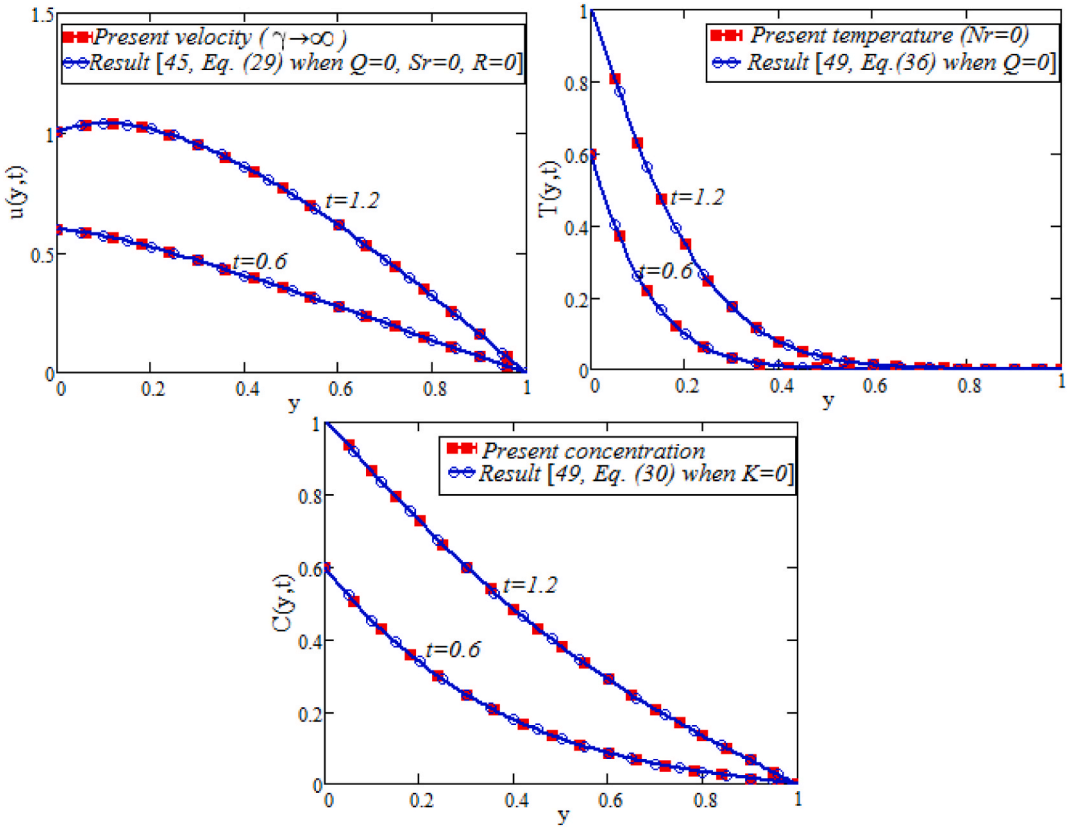

Fig. 8. Comparison of results with [49].

CRediT author statement

Conceptualization, Imran Siddique and Kashif Sadiq; methodology, Fahd Jarad and Imran Siddique; writing—original draft preparation, Kashif Sadiq; Funding acquisition, Mohammed M. M. Jaradat; Formal analysis, Fahd Jarad; Validation, Mohammed M. M. Jaradat; Software, Rifaqat Ali; writing—;review and editing, Imran Siddique, Mohammed M. M. Jaradat and Rifaqat Ali; supervision, Imran Siddique. All authors have read and agreed to the published version of the manuscript.

Funding

This research received no external funding.

Declaration of competing interest

The authors declare that they have no known competing financial interests or personal relationships that could have appeared to influence the work reported in this paper.

Acknowledgement

The authors would like to express the gratitude to Deanship of Scientific Research at King Khalid University, Saudi Arabia for providing funding research group under the research grant number R.G.P. 2/51/43. Open Access funding provided by the Qatar National Library.

References

[1] N. Casson, A Flow Equation for Pigment-Oil Suspensions of the Printing Ink Type, Rheology of Disperse Systems, pergamon press, London, UK, 1959.
[2] R.K. Dash, K.N. Mehta, G. Jayaraman, Casson fluid flow in a pipe filled with a homogenous porous medium, Int. J. Eng. Sci. 34 (10) (1996) 1145–1156.
[3] K.F.V. Wong, O.D. Leon, Applications of nanofluids: current and future, Adv. Mech. Eng. (2010) 1–11.
[4] S.U.S. Choi, J.A. Eastman, Enhancing thermal conductivity of fluids with nanoparticles, in: The Proceedings of the 1995 ASME International Mechanical Engineering Congress and Exposition vol. 66, ASME, FED 231/MD, San Francisco, USA, 1995, pp. 99–105.
[5] M. Sheikholeslami, M. Jafaryar, A. Shafee, Z. Li, A. Smida, I. Tlili, Heat transfer simulation during charging of nanoparticle enhanced PCM within a channel, Phys. Stat. Mech. Appl. 525 (2019) 557–565.

[6] R. Kandasamy, T. Hayat, S. Obaidat, Group theory transformation for Soret and Dufour effects on free convective heat and mass transfer with thermophoresis and chemical reaction over a porous stretching surface in the presence of heat source/sink, Nucl. Eng. Des. 241 (2011) 2155–2161.
[7] K. Das, Flow and heat transfer characteristics of nanofluids in a rotating frame, Alex. Eng. J. 53 (3) (2014) 757–766.
[8] S.A.A. Jan, F. Ali, N.A. Sheikh, I. Khan, M. Saqib, M. Gohar, Engine oil based generalized brinkman-type nano-liquid with molybdenum disulphide nanoparticles of spherical shape: atangana-Baleanu fractional model, Numer. Methods Part. Differ. Equ. 22200 (2017) 1–23.
[9] P. Loganathan, C.P. Nirmal, P. Ganesan, Radiation effects on an unsteady natural convective flow of a nanofluid past an infinite vertical plate, Nano 1 (2013) 1–10.
[10] M.G. Reddy, M.V.V.N.L. Sudharani, K.G. Kumar, An analysis of dusty slip flow through a single-/multi-wall carbon nanotube, Continuum Mech. Therm. 32 (2020) 1.
[11] M. Archana, M.M. Praveena, K.G. Kumar, S.A. Shehzad, M. Ahmad, Unsteady squeezed Casson nanofluid flow by considering the slip condition and time-dependent magnetic field, Heat Trans. 49 (8) (2020) 4907–4922.
[12] M.G. Reddy, M.V.V.N.L. Sudha Rani, M.M. Praveen, K.G. Kumar, Comparative study of different non-Newtonian fluid over an elaborated sheet in the view of dual stratified flow and ohmic heat, Chem. Phys. Lett. 784 (2021), 139096.
[13] M.G. Reddy, N. Kumar R, B.C. Prasannakumara, N.G. Rudraswamy, K.G. Kumar, Magnetohydrodynamic flow and heat transfer of a hybrid nanofluid over a rotating disk by considering Arrhenius energy, Commun. Theor. Phys. 73 (4) (2021), 045002.
[14] K.G. Kumar, E.H.B. Hani, M. El Haj Assad, M. Rahimi-Gorji, S. Nadeem, A novel approach for investigation of heat transfer enhancement with ferromagnetic hybrid nanofluid by considering solar radiation, Microsyst. Technol. 27 (2021) 97–104.
[15] M.G. Reddy, K.G. Kumar, S.A. Shehzad, A static and dynamic approach of aluminum alloys (AA7072-AA7075) over a semi-infinite heated plate, Phys. Scripta 95 (2020), 125201.
[16] B. Souayeh, K.G. Kumar, M.G. Reddy, Sudha Rani, N. Hdhiri, H. Alfannakh, M. Rahimi-Gorji, Slip flow and radiative heat transfer behavior of Titanium alloy and ferromagnetic nanoparticles along with suspension of dusty fluid, J. Mol. Liq. (2019), 111223.
[17] M.G. Reddy, M.V.V.N.L. Sudha Rani, K.G. Kumar, B.C. Prasannakumar, H.J. Lokesh, Hybrid dusty fluid flow through a Cattaneo–Christov heat flux model, Phys. Stat. Mech. Appl. 551 (2020), 123975.
[18] K.G. Kumar, M.G. Reddy, S.A. Shehzad, F.M. Abbasi, A least square study on flow and radiative heat transfer of a hybrid nanofluid in a moving frame by considering a spherically-shaped particle, Revista Mexicana de F'ısica 66 (2) (2019) 162–170.
[19] Y. Meng, F. Su, Y. Chen, Supercritical fluid synthesis and tribological applications of silver nanoparticle-decorated graphene in engine oil nanofluid, Sci. Rep. 6 (2016) 31246.
[20] V. Eswaraiah, V. Sankaranarayanan, S. Ramaprabhu, Graphene-based engine oil nanofluids for tribological applications, ACS Appl. Mater. Interfaces 3 (11) (2011) 4221–4227.
[21] S. Aman, M.Z. Salleh, Z. Ismail, I. Khan, Exact solution for heat transfer free convection flow of Maxwell nanofluids with graphene nanoparticles, J. Phys. Conf. 890 (2017), 012004.
[22] M. Arif, F. Ali, N.A. Sheikh, I. Khan, Enhanced heat transfer in working fluids using nanoparticles with ramped wall temperature: applications in engine oil, Adv. Mech. Eng. 11 (2019), 1687814019880987.
[23] B. Radisavljevic, A. Radenovic, J. Brivio, I.V. Giacometti, A. Kis, Single-layer MoS_2 transistors, Nat. Nanotechnol. 6 (3) (2011) 147–150.
[24] B. Radisavljevic, M.B. Whitwick, A. Kis, Integrated circuits and logic operations based on single-layer MoS_2, ACS Nano 5 (12) (2011) 9934–9938.
[25] I. Khan, Shape effects of MoS_2 nanoparticles on MHD slip flow of molybdenum disulfide nanofluid in a porous medium, J. Mol. Liq. 233 (2017) 442–451.
[26] Y. Zhang, S. Gu, B. Yan, J. Ren, Solvent-free ionic molybdenum disulfide (MoS_2) nanofluids, J. Mater. Chem. 22 (30) (2012) 14843–14846.
[27] S. Das, H.Y. Chen, A.V. Penumatcha, J. Appenzeller, High-performance multilayer MoS_2 transistors with scandium contacts, Nano Lett. 13 (1) (2012) 100–105.
[28] A. Dankert, L. Langouche, M.V. Kamalakar, S.P. Dash, High-performance molybdenum disulfide (MoS_2) field-effect transistors with spin tunnel contacts, ACS Nano 8 (1) (2014) 476–482.
[29] S. Gu, Y. Zhang, B. Yan, Solvent-free ionic molybdenum disulfide (MoS_2) nanofluids with self-healing lubricating behaviors, Mater. Lett. 97 (2013) 169–172.
[30] H. Kato, M. Takama, Y. Iwai, K. Washida, Y. Sasaki, Wear and mechanical properties of sintered copper-tin composites containing graphite or molybdenum disulfide, Wear 255 (1) (2003) 573–578.
[31] C. Mao, Y. Huang, X. Zhou, H. Gan, J. Zhang, Z. Zhou, The tribological properties of nanofluid used in minimum quantity lubrication grinding, Int. J. Adv. Manuf. Technol. 71 (5–8) (2014) 1221–1228.
[32] J. Liu, G.M. Choi, D.G. Cahill, Measurement of the anisotropic thermal conductivity of molybdenum disulfide (MoS_2) by the time-resolved magneto-optic Kerr effect, J. Appl. Phys. 116 (23) (2014), 233107.
[33] Y. Ding, B. Xiao, Thermal expansion tensors, Grüneisen parameters and phonon velocities of bulk MT 2 (M= W and Mo; T= S and Se) from first principles calculations, RSC Adv. 5 (24) (2015) 18391–18400.
[34] D.C. SobralFilho, A new proposal to guide velocity and inclination in the ramp protocol for the treadmill ergometer, Arq. Bras. Cardiol. 81 (1) (2003) 48–53.
[35] N. Ahmed, M. Dutta, Transient mass transfer flow past an impulsively started infinite vertical plate with ramped plate velocity and ramped temperature, Int. J. Phys. Sci. 8 (7) (2013) 254–263.
[36] F. Ali, M. Arif, I. Khan, N.A. Sheikh, M. Saqib, Natural convection in polyethylene glycol based molybdenum disulfide nanofluid with thermal radiation, chemical reaction and ramped wall temperature, Intern. J. Heat Tech. 36 (2) (2018) 619–631.
[37] G.S. Seth, M.S. Ansari, R. Nandkeolyar, MHD natural convection flow with radiative heat transfer past an impulsively moving plate with ramped wall temperature, Heat Mass Tran. 47 (5) (2011) 551–561.
[38] T.T. Kao, Laminar free convective heat transfer response along a vertical flat plate with step jump in surface temperature, Lett. Heat Mass Tran. 2 (5) (1975) 419–428.
[39] G. Seth, S. Hussain, S. Sarkar, Hydromagnetic natural convection flow with heat and mass transfer of a chemically reacting and heat absorbing fluid past an accelerated moving vertical plate with ramped temperature and ramped surface concentration through a porous medium, J. Egypt Math. Soc. 23 (2015) 197–207.
[40] G. Seth, R. Sharma, S. Sarkar, Natural convection heat and mass transfer flow with hall current, rotation, radiation and heat absorption past an accelerated moving vertical plate with ramped temperature, J. Appl. Fluid Mech. 8 (2015) 7–20.
[41] G. Seth, S. Sarkar, MHD natural convection heat and mass transfer flow past a time dependent moving vertical plate with ramped temperature in a rotating medium with Hall effects, radiation and chemical reaction, J. Mech. 31 (2015) 91–104.
[42] P. Chandran, N.C. Sacheti, A.K. Singh, Natural convection near a vertical plate with ramped wall temperature, Heat Mass Tran. 41 (2005) 459–464.
[43] M. Arif, P. Kumam, W. Kumam, I. Khan, M. Ramzan, A fractional model of Casson fluid with ramped wall temperature: engineering applications of engine oil, Comput. Math. Methods 3 (6) (2021) e1162.
[44] M. Ramzan, M. Nazar, Z.U. Nisa, M. Ahmad, N.A. Shah, Unsteady free convective magnetohydrodynamics flow of a Casson fluid through a channel with double diffusion and ramp temperature and concentration, Math. Methods Appl. Sci. (2021) 1–20.
[45] K. Sadiq, I. Saddique, J. Awrejcewicz, M. Bednarek, Natural convection water/glycerin-CNT fractionalized nanofluid flow in a channel with isothermal and ramped conditions, Nanomaterials 12 (2022) 1255.
[46] S. Kakaç, A. Pramuanjaroenkij, Review of convective heat transfer enhancement with nanofluids, Int. J. Heat Mass Tran. 52 (2009) 3187–3196.
[47] H.F. Oztop, E. Abu-Nada, Numerical study of natural convection in partially heated rectangular enclosures filled with nanofluids, Int. J. Heat Fluid Flow 29 (5) (2008) 1326–1336.
[48] F. Ali, B. Aamina, I. Khan, N.A. Sheikh, M. Saqib, Magnetohydrodynamic flow of Brinkman-type engine oil based MoS_2-nanofluid in a rotating disk with Hall Effect, Intern. J. Heat Tech. 35 (4) (2017) 893–902.
[49] K. Sadiq, I. Siddique, R. Ali, F. Jarad, Impact of ramped concentration and temperature on MHD Casson nanofluid flow through a vertical channel, J. Nanomater. (2021), 3743876.